Full Paper

Propellants, Explosives, Pyrotechnics

DOI: 10.1002/prep.201900214

Prediction of Probabilistic Detonation Threshold via Millimeter-Scale Microstructure-Explicit and Void-Explicit Simulations

Christopher Miller,[a] David Kittell,[b] Cole Yarrington,[b] and Min Zhou*[a]

Abstract: We present an approach and relevant models for predicting the probabilistic shock-to-detonation transition (SDT) behavior and Pop plot (PP) of heterogeneous energetic materials (HEM) via mesoscopic microstructure-explicit (ME) and void explicit (VE) simulations at the millimeter (mm) sample size scale. Although the framework here is general, the particular material considered in this paper is pressed Octahydro-1,3,5,7-tetranitro-1,2,3,5-tetrazocine (HMX). To systematically delineate the effects of material heterogeneities, four material cases are considered. These cases are homogeneous material, material with granular microstructure but no voids, homogeneous material with voids, and material with both granular microstructure and voids. Statistically equivalent microstructure sample sets (SEMSS) are generated and used. Eulerian hydrocode simulations explicitly resolve the material heterogeneities, voids, and the coupled mechanical-thermal-chemical processes. In particular, it is found that both microstructure and voids strongly influence the SDT behavior and PP. The effects of different combinations of microstructure heterogeneity and voids on the SDT process and PP are quantified and rank-ordered. The overall framework uses the Mie–Grüneisen equation of state and a history variable reactive burn model (HVRB). A novel probabilistic representation for quantifying the PP is developed, allowing the calculation of (1) the probability of observing SDT at a given combination of shock pressure and run distance, (2) the run-distance to detonation under a given combination of shock pressure and prescribed probability, and (3) the shock pressure required for achieving SDT at a given run distance with a prescribed probability. The results are in agreement with general trends in experimental data in the literature.

Keywords: HMX · detonation · probabilistic · CTH · shock

1 Introduction

One of the longstanding challenges within the field of energetic materials is making accurate predictions of macroscopic ignition safety as well as performance, using fundamental material attributes at lower size scales. For a high-speed impact scenario (~ km/s), it is desirable to know what the likelihood is for ignition to occur – this assessment relates to safety and reliability. On the other hand, it is also important to quantify the minimum time and distance from the onset of impact to the development of steady state detonation – the shock-to-detonation transition (SDT). Given the broad range and variability of different impact scenarios, these assessments must be carried out under well-characterized conditions to allow applications to the varying scenarios via macroscopic state variables such as pressure, energy, loading rates, and distance. It is also understood that a heterogeneous energetic material (HEM) will exhibit greater sensitivity to shock than a corresponding homogeneous material, as material heterogeneities and defects enhance localized deformation, heating, failure, and chemical reactivity.

Specifically, the heterogeneous SDT process [1,2] is fundamentally different from what occurs during the shock initiation of a homogeneous explosive, such as liquid nitromethane [3] or hydrogen peroxide [4]. When homogeneous explosives are shocked, they are heated to a single bulk temperature immediately following the leading shock wave. When this bulk temperature is sufficiently high (i.e., for a thermal runaway to occur), a super-detonation wave forms in the material that was held at elevated temperatures the longest [5], usually near the interface between a homogeneous explosive and a projectile/impactor. The super-detonation wave must overtake the leading shock before a steady detonation is reached. Consequently, this initiation mechanism underlies the reason as to why homogeneous explosives appear as relatively shock insensitive compared to heterogeneous ones; a critical ignition temperature must be reached during the initial shock or impact that is based

[a] *C. Miller, M. Zhou*
Woodruff School of Mechanical Engineering
Georgia Institute of Technology
801 Ferst Dr, Atlanta, GA, 30332
**e-mail: min.zhou@gatech.edu*
[b] *D. Kittell, C. Yarrington*
Sandia National Laboratories
Albuquerque, New Mexico 87185

on the chemical activation energy (and it is typically higher for solids than liquids). Over the times and distances associated with the SDT process, homogeneous explosives are mostly treated with continuum modeling approaches, using the appropriate mixture theories and rate laws [6].

In contrast, when a heterogeneous explosive is shocked, the SDT process is dominated by the details of the heterogeneous microstructure that lead to heterogeneous reactions. A homogenized continuum model treatment would be unable to capture detailed material information at scales below the resolution of the computational elements or cells. In such a case, the average (shocked) bulk temperature would be too low for a super-detonation wave to occur (e.g., see [7]); however, it is known that material heterogeneities can cause energy to be localized into regions known as hot spots [8] – it is at these sites where the chemical reaction begins. A successful, heterogeneous SDT results in the more gradual build-up of reaction behind the leading shock wave, which then strengthens the leading shock until it transitions to a detonation wave without any overshoot.

Thus, a pressed, porous explosive is more sensitive to shock and it will detonate in less time and distance than a pure explosive crystal or homogeneous liquid explosive under similar loading conditions. The increased sensitivity of HEMs is a direct result of the shock wave interactions with the heterogeneous microstructural features such as small cracks, voids, and discontinuities in the forms of boundaries and interfaces between constituents (binders, grains, metal particles, and oxidizer granules). These microstructural features can be unique for certain HEMs, and result from available manufacturing and processing methods that must be employed. Typically, microstructural features range in size from tens of nm to hundreds of μm, and sometimes even as large as mm. For SDT, these features play a critical role in determining the explosive's shock sensitivity. For example, Welle et al. showed an empirical link between the microstructure and shock initiation behavior of neat HMX [9] via the class of the material (class III vs. V). The existence of this kind of a link was previously hypothesized by Baer [10] who used realistic three-dimensional HEM microstructures in a hydrocode simulation. Hence, both experiments and computations indicate that the overall SDT behavior is influenced by the processes occurring at the meso or grain scale.

Despite such general knowledge that HEM microstructures localize shock wave energy to form hot spots, there is little consensus as to the relative importance of the different hot spot mechanisms, or as to which mechanisms are active in different loading and material regimes. The hydrodynamic hot spot model, as introduced by Mader [11], was one of the very first to consider pore collapse and jet impingement following a shock wave; this raises the local temperature higher than the bulk (i.e., Hugoniot) temperature. However, more recent pore collapse models by Austin et al. [12] show that the inclusion of a viscoplastic crystal model will lead to shear banding and chemical reaction around the site of the pore. Regardless of the fidelity and type of the different models used, all direct numerical simulations (DNS) of shock-induced hot spots still require an explicit representation of the material microstructure. With current progress in the field, it is now possible to calculate the interactions of shocks with a much larger volume of the microstructure, which has led to a flurry of recent publications surrounding mesoscale modeling of explosives initiation (MMEI) [13–19]. Historically, these mesoscale simulations were carried out at the micron-scale, with the aim of predicting the effects that the microstructure has on the shock response of the material. However, this scale is much smaller than the scale of the full SDT process, which is observed over a few mm and may take several microseconds to complete. In addition, this scale is also well below the scale of heterogeneities on the order of hundreds of microns or even mm as noted earlier of many common HEMs.

To summarize some of the recent MMEI efforts aimed at shock initiation, Handley et al. [13] published a review article that encapsulates the mesoscale modeling approach; the review also includes many of the advances made through 2017. Yet, in attempting to translate all of the lessons learned from mesoscale modeling to the next higher scale (i.e., continuum burn models), several gaps were identified that remain unsolved to this day. Note that continuum reactive burn models do not currently treat the mechanisms of ignition or hot spot evolution directly. Elsewhere, Rai and Udaykumar [14] have demonstrated the feasibility of an image to computation approach for mesoscale simulations of HMX, using detailed material models and chemistry based on the Henson-Smilowitz multi-step kinetic mechanism. Their mesoscale simulations show that hot spots may or may not lead to initiation, based on whether the HMX is class III or V. However, this ignition behavior is sub-detonative, and it does not yet represent the full SDT process. Other mesoscale studies have looked at these same differences between class III vs. class V HMX in high-speed impact scenarios. For example, Kim et al. [15, 16] employed a framework based on the Lagrangian cohesive finite element method (CFEM) that has been shown to be able to produce probabilistic ignition criteria in James space, with the same trends found in the experiments. This capability is especially useful for predicting go/no-go thresholds, but it does not treat the full SDT transition, and instead focuses on hot spot evolution and the criticality condition for thermal runaway.

Other recent approaches to mesoscale modeling include work by Jackson et al. [17], which utilizes a density-based kinetics model, and a power deposition term in the energy equation to phenomenologically represent discrete hot spots. Comparison studies are also given to show the relative importance of the number density of hot spots, the microstructure of the crystalline pack, and other numerical parameters. In addition, Wood et al. [18] examined the role that the constitutive model plays in a mesoscale calculation

by using the atomistic code, LAMMPS, to train a strain rate-dependent SGL viscoplastic strength model. Two mesoscale simulations were then run with and without the SGL model turned on (i.e., hydrodynamic only), where it was found that an increase in the shocked temperature distribution occurs at lower impact velocities (less than ~1 km/s) if the SGL model is in use. Hence, strong shock initiation (i.e., several GPa of pressure) is most likely a purely hydrodynamic process. Finally, Yarrington et al. [19] have shown the full SDT process for a pressed porous explosive with nanoscale features in two dimensions. These large Eulerian calculations make use of a representative microstructure and a tuned Arrhenius-type burn model to match experimental results. Although the full computational domain was never shown in the paper, the run-to-detonation simulations employed a two-dimensional, 10 μm by 200 μm rectangular mesh with a total aspect ratio of 20:1 (which is among the highest aspect ratios ever published). These simulations also consisted of 80 million finite volume elements. Such large computational domain sizes appear to be more accessible in a pure Eulerian hydrocode, rather than one that is Lagrangian or arbitrary Lagrangian-Eulerian (ALE). Yet, there are still advantages and disadvantages to all three types of numerical methods.

In the current work, the nature of HEM shock initiation safety is explored for HMX using a new computational framework; one that explicitly resolves microstructures, voids, and chemical reaction at the millimeter scale. These are mesoscale microstructure-explicit (ME), void-explicit (VE), and chemical-reaction-explicit (CRE) simulations performed with the Eulerian hydrocode CTH [20]. The objective is to show the SDT transition for the first time as a probability distribution map overlaid on a Pop plot, with the source of uncertainty being material heterogeneities. As described by Dick et al. [21], the Pop plot originated from shock initiation studies which varied the shock pressure input to a HEM with an explosive lens/attenuator. The response measure is the run distance to detonation recorded via a streak camera. The shock pressure vs run distance plot is usually in the log-log space and called the Pop plot (PP). Here, the probabilistic Pop plot (PPP) represents a further step beyond previous studies by Kim et al. that have predicted a probabilistic ignition threshold in the James space [15, 16]. Randomized microstructural generation is employed in addition to explicit modeling of the void distributions in order to quantify their rank-order effects on the total run distance to detonation. The probabilistic analysis is made possible via the generation and use of statistically equivalent microstructure sample sets (SEMSS). The multiple samples in a specific material set directly mimic the multiple samples in experiments, allowing statistical variations in material and material response to be studied [15, 16].

The ME and VE simulations shown in this work not only resolve the material heterogeneities at the millimeter scale, they also capture the probabilistic nature of the SDT process. In these simulations, the constitutive relations are based on a simplified form of the SGL model, following recent success at calibrating this model in CTH [18]. Finally, a simplified reaction model is used to represent each of the individual HMX grains. This preliminary reaction model follows the work of Baer [10], which has been used in the absence of a more physically-relevant reaction model and equation of state (EOS) that are not currently available in CTH. The two-state history variable reactive burn model (HVRB), used here, has led to good agreement with experimental run distance to detonation and other continuum-level measurements in the past [10], and features a reaction rate that is based on local pressure. With these model assumptions, the shock to detonation transition events are set in motion by loading effected with an imposed piston velocity. This approach is often used to analyze the full SDT events on modern computing resources [22, 23].

Overall, the objectives of this work seek to develop a novel probabilistic representation for quantifying the shock sensitivity of HEMs. While the data sets used here to determine the parameters in the probabilistic representation come from computational simulations with the SEMSS, the probabilistic formulation can also be parameterized using independent experimental data sets. The results allow the determination of the likelihood of observing SDT at a particular run distance under a given shock pressure. This further advance is based on, but goes beyond the previous work of Kim et al. on thermal runaway and probabilistic ignition thresholds [15, 16]. In order to achieve this desired outcome, a new non-dimensionalized Pop plot characteristic parameter (called the Pop plot number) is proposed. The different effects of microstructure and voids on the probabilistic Pop plots are given in rank-order to gain insight into the meso (grain) scale mechanisms that underlie the SDT process. While current results pertain only to HMX, this approach could easily be repeated for other HEMs which are either synthesized in a traditional manner or additively manufactured. The remaining paper consists of two parts. The first part describes the computational framework used to study SDT at the mesoscale, including the design of the HMX microstructures, constitutive relationships, and reaction model. The second part discusses the simulation results, focusing on the rank-order of the effects of different microstructural features as well as the development of the probabilistic Pop plot. The paper concludes with major findings as well as directions for future work.

2 Framework of Analysis

Two-dimensional microstructures are generated and used. The impact loading is effected with a rigid piston traveling at different velocities. The run distance to detonation is calculated as the simulation progresses. The Sandia National Labs Eulerian hydrocode, CTH, is used to simulate the full

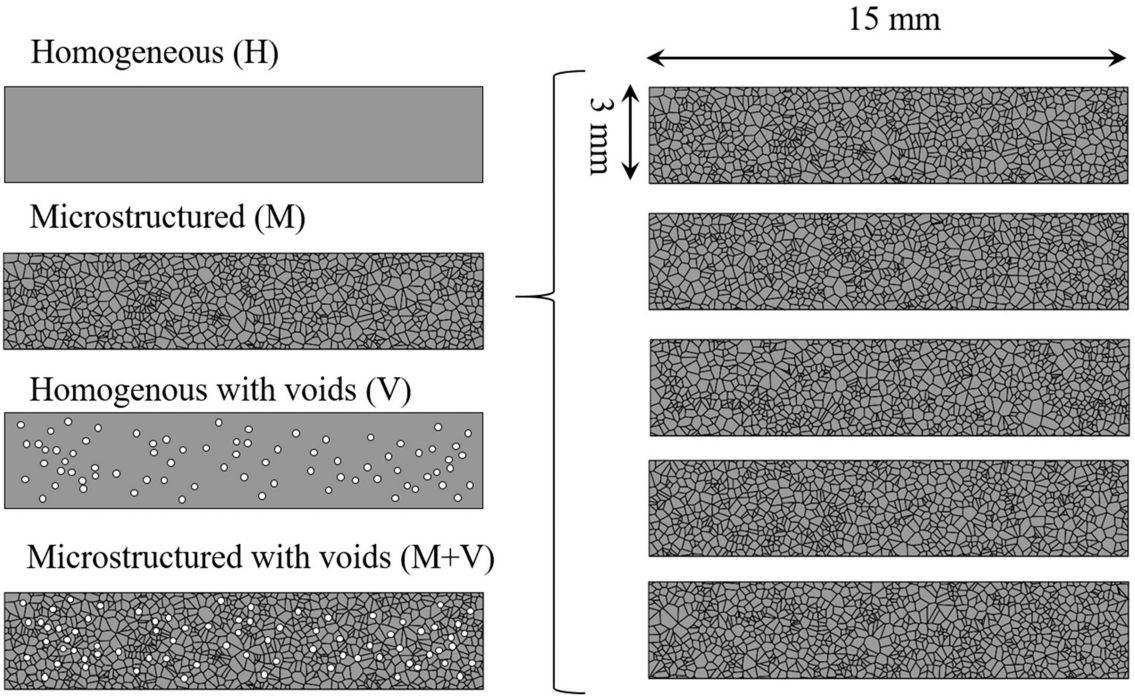

Figure 1. Four HMX material cases considered in this study: homogeneous (H), microstructured (M), homogeneous with voids (V), and microstructured with voids (M + V). Multiple, randomized grain morphologies and void placements were generated to create the four statistically equivalent microstructure samples sets (SEMSS) for analysis.

SDT process. The microstructure generation, constitutive relations, and computational framework are outlined in this section.

2.1 Material, Model and Microstructure

The material of interest is approximately based on class III pressed granular HMX [9]. Four types of models are considered: homogenous (H), microstructured without voids (M), homogenous with voids (V), and microstructured with voids (M + V), as shown in Figure 1. The homogeneous (H) and microstructured (M) samples are fully-dense (100% TMD). The voids in the V and M + V samples are circular in shape and have diameters of 50 μm. This void size is chosen to allow explicit resolution of each void in the 3 × 15 mm samples without rendering the already very intensive computations prohibitively expensive using 10,000–20,000 processor hours on supercomputers. Further discussions on mesh size and computational cost are in section 2.4. Section 3.1 studies the effect of void volume fractions ranging from 0% to 20%, while section 3.2 compares the effects of granular microstructure without voids relative to samples with 5% volume fraction of voids.

A set of five random but statistically similar granular HMX microstructures is generated using Voronoi tessellation. These samples conform to the statistical grain size distribution in Figure 2. This grain size distribution is monomodal, with a mean grain diameter of 229 μm. This method of microstructure generation results in realistic, randomized, and statistically equivalent microstructure sample sets (SEMSS). For samples with voids, individual voids are inserted randomly into either the homogenous or microstructure samples until the overall desired void volume fraction (0%, 5%, 10%, or 20%) has been reached. No two voids overlap, ensuring a constant void size and random void distribution.

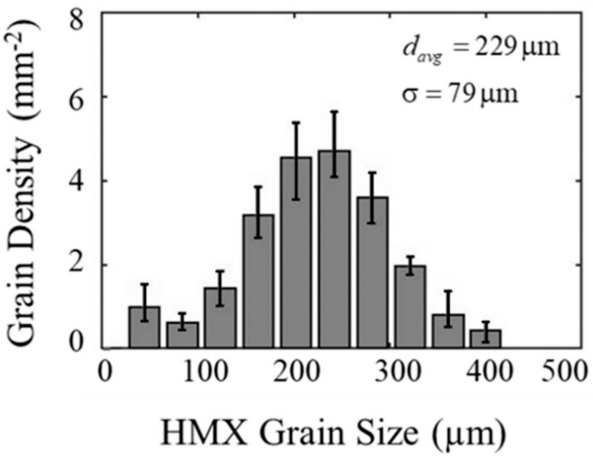

Figure 2. Monomodal HMX grain size distribution used in the granular microstructures with and without voids.

Actual samples in experiments have more heterogeneous characteristics than those in the four sets of samples presented here. For example, nano- and micro-scale voids, microcracks, and directionality of the material properties due to the anisotropic nature of the HMX crystal all play roles in the response of the materials to shock loading. These factors are too small and computationally expensive to be explicitly resolved in the current model setting. To account for the effects of these factors via grain-level heterogeneities, the density of the HMX for each grain is set to one of three possible values: 70% TMD (1.33 g/cm^3), 100% TMD (1.90 g/cm^3), and 130% TMD (2.47 g/cm^3). These density variations emulate the effects of local variations in the material and represent one source of variations in fields behind the shock front normally attributed to localized material heterogeneities. Such variations lead to the heterogeneous behavior as seen in actual samples, thereby enabling a probabilistic analysis described later in this paper, while keeping the overall HMX density consistent at 100% TMD. A variation of 30% about the 100% TMD was calibrated based on the work of Hardin et al. [24] who found the coefficient of variation in the longitudinal stress field in the quasi-steady region behind the stress wave front in polycrystalline HMX varies from 0.08 to 0.16 at piston velocities around 400 m/s. In this study, the grains are assumed to be perfectly bonded to one another. If two grains with the same density are positioned next to one another, they behave as a single grain of the same density. For the H and V samples, the standard HMX 100% TMD (1.90 g/cm^3) is used.

The present framework represents a simplified approach toward explicitly resolving various microstructures commonly seen in HEM. While the method of varying the density of the HMX grains may replicate the trends seen in experiments, it is difficult to fully quantify the effect of heterogeneity into a single parameter. Actual experimental samples have clear defects not accounted for here, which are known to contribute to hotspot initiation and subsequent detonation [16,25–27]. Other HEMs have binder and additive components, such as aluminum, which can affect the sensitivity of the material to ignition [28]. It is entirely possible that microstructure heterogeneity plays an even larger role than what is presented in the results of this study. However, the current framework should be regarded as a step toward fully accounting for the most essential material heterogeneities up to the overall mm macroscopic size scale.

2.2 Constitutive Relations

The elastic-viscoplastic model, equation of state (EOS), and chemistry model are most relevant to the community and the analyses here. Consequently, they are discussed in this section. The specimen is initially stress-free and at rest. This is a 2D model and the conditions of plane-strain prevail. A single piston velocity (U_P) is applied on one end of the sample to effect shock loading. The side (lateral) boundaries are constrained in a frictionless manner to maintain the overall conditions of sample-level uniaxial strain typical of planar impact experiments.

A simplified Steinberg-Guinan-Lund strain-dependent flow stress model (SGL) is used to account for the viscoplastic behavior of HMX. This strain-rate dependent model is well-suited for high strain-rate deformation and accounts for the effects of thermal softening. The material yield stress is calculated via

$$\sigma_Y(\dot{\varepsilon}_P, T) = [\sigma_A + \sigma_T(\dot{\varepsilon}_P, T)], \tag{1}$$

with

$$\dot{\varepsilon}_P = \left\{ \frac{1}{C_1} \exp\left[\frac{2U_K}{T} \left(1 - \frac{\sigma_T}{\sigma_P} \right)^2 \right] + \frac{C_2}{\sigma_T} \right\}^{-1}. \tag{2}$$

In the above relations, σ_A is the athermal component of the flow stress, σ_T is the thermally activated component of the flow stress, and C_1, C_2, U_K, and σ_P are material parameters. The model has been calibrated to match the elasto-viscoplastic model used for HMX by Kim et al. [15] which in turn was based on available experimental data. The values of the material parameters in the model are listed below in Table 1.

The bulk response to hydrostatic pressure is modeled using the first order Mie–Grüneisen EOS

$$p = \frac{\rho_0 C_0^2 \left(1 - \frac{\rho_0}{\rho}\right) \left[1 - \frac{\Gamma_0}{2}\left(1 - \frac{\rho_0}{\rho}\right)\right]}{\left[1 - s\left(1 - \frac{\rho_0}{\rho}\right)\right]^2} + \rho_0 \Gamma_0 E, \tag{3}$$

where p is the pressure, ρ_0 is the initial density of HMX, ρ is the current density of HMX, Γ_0 is the Grüneisen parameter, C_0 is the bulk sound speed, and s is the slope of the Hugoniot. E is the internal energy which is found by integrating the specific heat with respect to temperature at constant volume, i.e.,

$$E = \int_0^T c_v dT. \tag{4}$$

The HMX material parameters for the Mie–Grüneisen EOS model are listed in Table 2.

The process of chemical reaction initiation and progression follows the HVRB in the form of

Table 1. HMX material parameters for SGL flow stress model.

C_1	C_2	U_K	σ_P	σ_A
3.79×10^{11} s^{-1}	1.45 Pa·s	3000 K	650 MPa	260 MPa

Table 2. HMX material parameters for the Mie-Grüneisen EOS model.

ρ_0	C_0	s	Γ_0
1.33 g/cm^3 or 1.90 g/cm^3 or 2.47 g/cm^3	2900 m/s	2.0	1.0

$$\lambda = 1 - \left(1 - \frac{\phi^M}{X}\right)^X, \tag{5}$$

where

$$\phi = \tau_0^{-1} \int_0^t \left[\frac{(p - p_i)}{p_R}\right]^Z dt. \tag{6}$$

In the above relations, λ is the extent of reaction, τ_0 is a scaling constant, p is the current pressure, p_i is the threshold pressure for reaction, andp_R, X, M, and $Z$are reaction rate parameters. Reactive burn models have been widely used to simulate the ignition and detonation of HEMs [10, 29, 30]. These empirical models are often calibrated to Pop plot data. As a result, the localized extent of reaction behind the shock front may not be perfectly resolved (which is a known limitation for the HVRB model). However, with available data and models, this is a reasonable trade-off in order to reach the macroscale from the mesoscale, since the focus here is on analyzing macroscale material behavior. The HVRB model provides a straightforward method of accounting for chemical reaction at larger size scales which would otherwise prove more computationally intensive if an Arrhenius-based chemical reaction rate model is used. Still, it is worthwhile to note that if and when a more useful chemistry model is made available, it can be easily used in the current framework – there is no fundamental impediment to the use of other, especially more mechanisms-based, reaction models. The calibration parameters shown in Table 3 have been fit to the average state data of pure HMX and are found in the CTH material properties library [31, 32].

2.3 Shock Pressure and Run Distance Calculation

Run distance to detonation is a common metric used to measure SDT sensitivity of an energetic material. In this analysis, the run distance to detonation is defined as the longitudinal distance the shock wave travels into the explosive before the detonation wave front is established. Initially, the stress field following the shockwave is relatively uniform (in the homogeneous samples), due to the monotonic loading applied. When voids or microstructure are introduced, the stress field deviates from this idealized scenario as the shock front encounters material heterogeneity. The reaction builds up behind the shock front, and at later times strengthens it before eventually overtaking the shock front and propagating through the uncompressed material as a detonation wave.

Table 3. HMX material parameters for the HVRB chemistry model [32].

τ_0	p_i	p_R	X	M	Z
1×10^{-6} s	500 MPa	6 GPa	1	1.5	2.36

The relationship between run distance to detonation and pressure of imposed shock loading, or the Pop plot, can be used to compare the relative shock sensitivity of different materials. In the analysis here, the relations are used to quantify the differences in shock initiation response due to microstructure and voids of the four HMX cases. The shock pressure is calculated based on the spatially averaged pressure profile of each sample. The initial plateau of the stress wave is measured and averaged over both sample distance and time in order to determine the most accurate monotonic shock pressure for a given impact velocity. In order to calculate the run distance, the location of the shock front in the sample is recorded as a function of time. Since the detonation wave propagates faster than the inert shock wave, the run distance is easily measured by examining the change in velocity of the shock front itself. An example pressure profile and shock front location of a granular microstructure without voids under loading by a piston velocity of $U_P = 800\,\mathrm{m/s}$ is shown in Figure 3.

The fields of pressure, temperature, and the extent of reaction (λ) are analyzed to delineate the effects of voids and granular heterogeneity. Figure 4 shows the pressure fields at different stages of the SDT process for a microstructured HMX sample with voids impacted by an aluminum flyer at 400 m/s. The fields cover hotspot initiation to full detonation completion.

2.4 Mesh and Size Convergence

To ensure accurate results, a mesh convergence study is carried out to determine the proper mesh size necessary to explicitly resolve both the grains and voids and ensure convergence of solution of interest. To this end, shock pressure and run distance are calculated for samples including both microstructure and voids at mesh sizes ranging from 30 μm to 500 nm. The M + V sample set was chosen for this purpose because it accounts for both kinds of heterogeneities. Naturally, the mesh sufficient for modeling the most complicated HMX microstructures should be sufficient for the less complicated microstructures as well. As shown in Figure 5, the shock pressure is found to converge at any resolution finer than 20 μm, while the run distance converges for any mesh size finer than 5 μm. For this reason, a final mesh size of 5 μm is chosen for all subsequent tests. It is important to note that this study is focused on the macro-

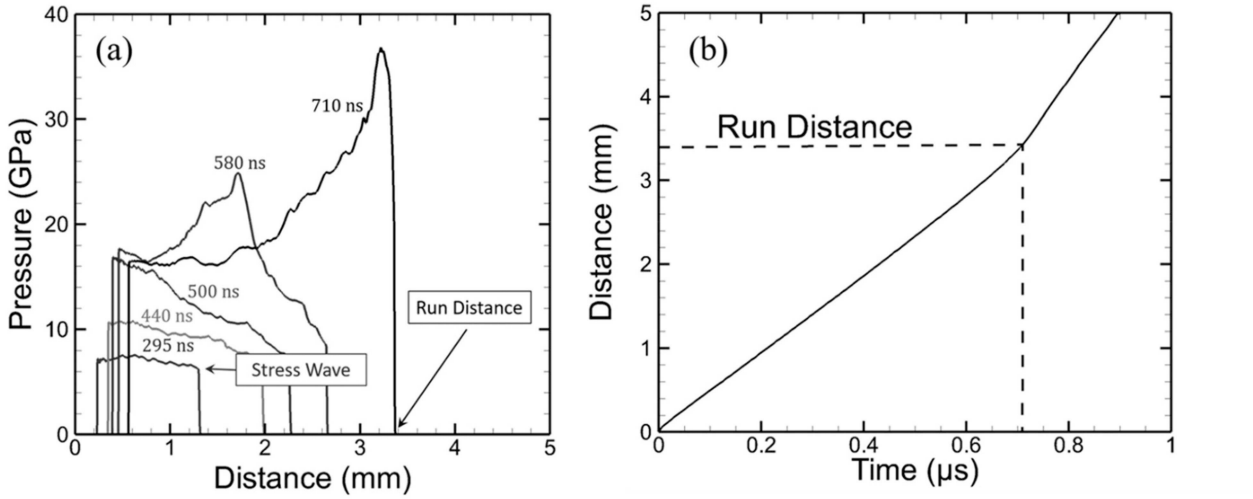

Figure 3. (a) Pressure profiles behind the shock front at multiple times for a microstructure sample impacted at $U_P = 800$ m/s. (b) Distance traversed by the shock front as a function of time for the same microstructure sample impacted at $U_P = 800$ m/s.

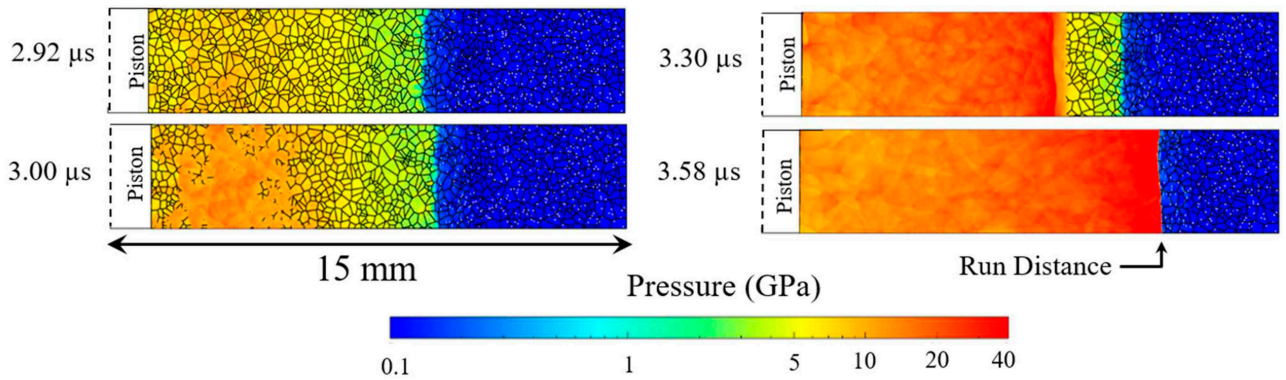

Figure 4. Pressure fields for an HMX sample containing both microstructure and voids impacted by an aluminum flyer at $U_P = 400$ m/s.

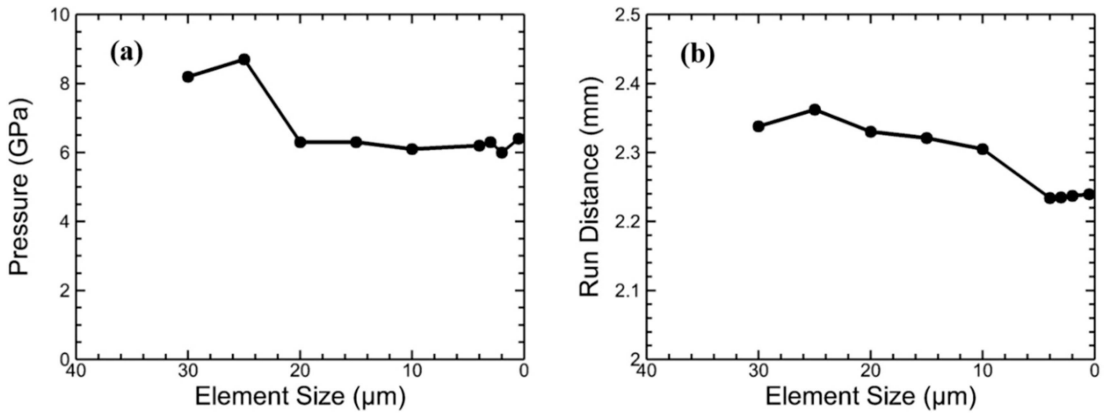

Figure 5. (a) Shock pressure and (b) run distance to detonation for a sample with granular microstructure and voids at mesh resolutions ranging from 30 μm elements to 500 nm elements.

scale detonation properties of the material. A finer mesh resolution would likely be required to accurately resolve local temperatures which may be required for an Arrhenius-based chemical reaction rate model, as is commonly used for small scale simulations in the literature. The HVRB chemical reaction model used here (as outlined in section 2.2) is a pressure-dependent model that does not require direct use of temperature. For this reason, the convergence study here also provides a validation of the average shock pressure.

In addition to a mesh resolution study, it is important to determine whether the sample size chosen serves as an acceptable representative volume element (RVE) for the microstructure as a whole. While the smallest microstructure feature (voids) dictates the necessary mesh resolution, the largest microstructure feature (grains) dictates the necessary RVE size of the sample. To this end, five 1 mm × 5 mm samples, with the same randomized grain distributions as in the 3 mm × 15 mm samples (see Figure 2), are subject to the same impact loading and the detonation process is analyzed in the same as manner as that in the 3 mm × 15 mm samples. The resulting shock pressure prior to detonation and the run distance to detonation are calculated. The results are shown in Figure 6. The overlap and near full coincidence of the data points from the two sets of samples indicate that the 1 mm × 5 mm sample size yields practically the same results as the 3 mm × 15 mm sample size, and therefore the 1 × 5 mm samples are large enough to be RVEs. For the remainder of this analysis, calculations are conducted using 1 mm × 5 mm samples to minimize computational cost.

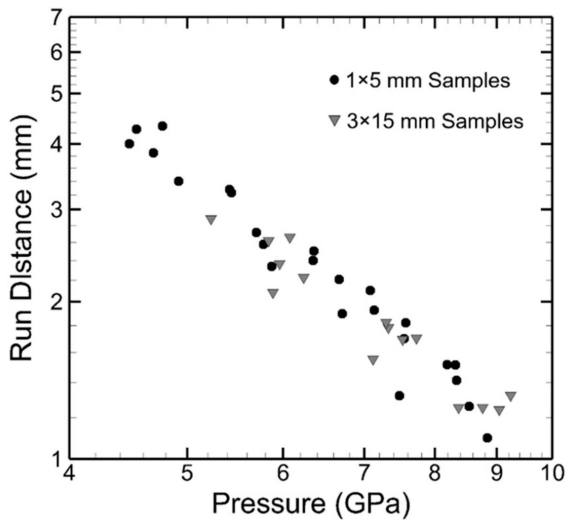

Figure 6. Run distance to detonation as a function of shock pressure for five 1 × 5 mm samples (circles) and five 3 × 15 mm samples (triangles) with randomized grain distributions and no voids. Piston velocities ranging from 600 m/s–1000 m/s are used to generate the range of shock pressures seen here.

3 Results and Discussion

A systematic quantification of the effect of granular microstructure and void volume fraction on the shock sensitivity of pressed HMX is carried out. Section 3.1 compares the effects of homogenous samples with four volume fractions of 50 μm circular voids (0%, 5%, 10%, and 20%) on the Pop plot. Section 3.2 discusses the differences in samples with and without voids and granular microstructure; a comparative rank-ordering of the Pop plot results is also given. A probabilistic model for the SDT transition is developed in section 3.3, using the results presented in section 3.2. This formulation allows the likelihood of achieving run to detonation at a given distance to be mapped over the entire range of loading pressure studied. Finally, in section 3.4 we compare the prediction obtained in section 3.2 with available experimental data.

3.1 Effects of Void Volume Fraction

It is well known that microstructural heterogeneities contribute to increased sensitivities of energetic materials to ignition. The presence of voids in the material results in extreme shear stress and local plastic deformation at the defect locations under shock loading conditions. The hotspot formations due to pore collapse are considered to play a dominate role in the sensitivity, and subsequent detonation of HEMs. Accurately characterizing the effects of voids is essential in mesoscale simulations [33]. In this section, we examine the effect of increasing the volume fraction of voids on the run distance to detonation of HMX samples without microstructure or other forms of heterogeneity.

Homogeneous HMX samples with four levels of void volume fractions are analyzed: 0% (homogeneous), 5%, 10%, and 20%. These values are chosen to track void volume fractions commonly observed in experiments of pressed HMX [34]. All voids are initially circular with the same diameter of 50 μm. The voids are placed randomly so that no two voids initially overlap or directly contact the edges of the sample. For each of the four void volume fractions, five statistically equivalent random samples are generated, resulting in five 5% void samples, five 10% void samples, and five 20% void samples. Each sample is subjected to loading at each of the following piston velocities: $U_P = 600$, 700, 800, 900, and 1,000 m/s. The use of multiple statistically equivalent samples over a range of piston velocities allows for measurement of both shock pressure and run distance in a manner that captures the stochastic variations in the material behavior. The results of this analysis are shown in Figure 7. Clearly, the run distance decreases as the void volume fraction increases. The average decrease in run distance with void volume fraction is normalized with respect to the 0% void case and is listed in Table 4.

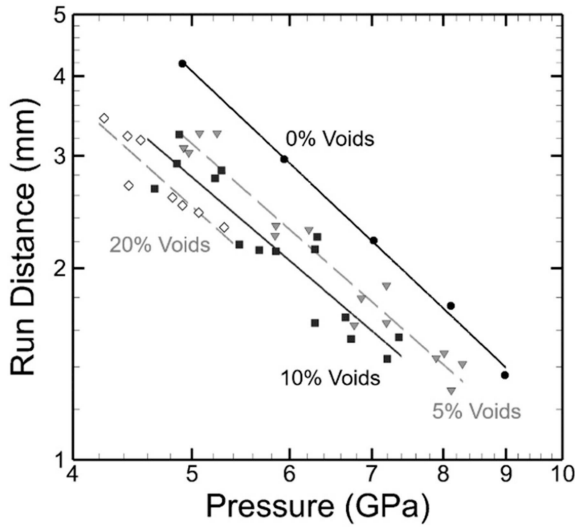

Figure 7. Pop plots of samples with 0% void (circles), 5% voids (triangles), 10% voids (squares), and 20% voids (diamonds) by volume. All voids are initially 50 μm in diameter. Other than the voids, the samples contain no other heterogeneities.

Table 4. Effect of void volume fraction on normalized run distance.

Void Volume Fraction	Average Decrease in Run Distance
0%	0%
5%	20.6%
10%	28.8%
20%	37.2%

For a given shock pressure, increasing the volume fraction of voids in turn causes the run distance to detonation to decrease (and therefore lowers the PP line). Table 4 shows that the rate of decrease in the run distance decreases at higher void volume fractions. Specifically, a 5% volume fraction of voids causes the run distance to decrease on average by 20.6% relative to the homogeneous material case over the entire range of shock pressure. Increasing the void volume fraction from 5% to 20%, on the other hand, causes the run distance decrease relative to the 0% case to change from 20.6% to 37.2%, a smaller 16.6% change. While increasing the volume fraction of voids lowers the Pop plot line, a trend that is associated with increased sensitivity of an HEM to shock, trade-offs must also be considered. Specifically, voids cause the overall effective density of the material to decrease, which leads to lower shock pressure under the same impact velocity. This means a higher, more severe loading might be required to generate the same performance or effect. In addition, voids also decrease the overall energy content in a HEM, causing the overall energy output per unit macroscopic volume of the material to be lower. These factors must be weighed.

3.2 Effects of Granular Heterogeneities

We now consider the effects of the granular microstructure, as well as the interactions between the effects of the microstructure and voids, on the Pop plot. For this purpose, the four material cases in Figure 2 are considered: homogeneous, granular microstructure only, voids only, and both microstructure and voids. The overall results are shown in Figure 8. As different forms of heterogeneities and material defects, microstructure and voids each causes the Pop plot lines to shift to the lower left in pressure-run distance space. In other words, the run distance decreases at a given shock pressure as more heterogeneities are included. The average decrease in run distance for each material case (H, M, V, M+V) has been normalized with respect to the homogeneous case (H), as listed in Table 5.

For the range of pressure considered, homogeneous samples have the highest Pop plot line or the longest run distance at a given pressure. Voids and granular microstructure each cause the Pop plot line to move toward the lower left in the shock pressure-run distance space. Rela-

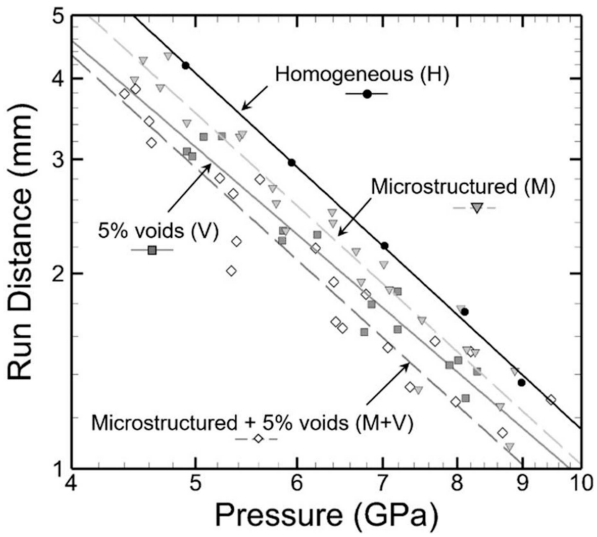

Figure 8. - Pop plot lines for the homogeneous samples (circles), granular microstructured samples (triangles), samples with 5% voids by volume only (squares), and samples with 5% voids and granular microstructure (diamonds).

Table 5. Effect of material heterogeneities on normalized run distance.

Sample Type	Average Decrease in Run Distance
Homogeneous (H)	0%
Microstructure (M)	12.3%
5% Voids (V)	20.6%
5% Voids and Microstructure (V+M)	27.5%

tively speaking, the effects of 5% voids are stronger than the effects of granular heterogeneities embodied by ±30% grain-grain variations in the density of the material. The Pop plot line for samples with both microstructure and voids have the lowest Pop plot line, or the fastest SDT in terms of run distance and time among the cases analyzed. The results in Tables 4 and 5 allow a rank-order of the effects of microstructure and voids to be established. A graphical illustration of this ordering is given in Figure 9. From the lowest to highest SDT sensitivity: homogenous HMX, HMX with only microstructure, HMX with 5% voids, HMX with 5% voids and microstructure, HMX with 10% voids, and HMX with 20% voids. Due to the significant amount of scatter in the M, V, and M+V data sets seen in Figure 8, the rank ordering presented here represents only an average decrease in run distance. Clearly a more probabilistic approach will be required to fully quantify the effects of heterogeneities. This new probabilistic analysis is discussed in Section 3.3.

For the 0% and 5% void cases, adding granular microstructure decreases the run distance by 12.3% and 6.9%, respectively. Clearly, microstructure has a significant effect on the SDT behavior and the Pop plot. It is important to point out that a relatively idealized microstructure representation is used here, as the only material heterogeneity is in the density (which in turn affects the EOS). In reality, material heterogeneities lie in constitutive behavior, crystal orientation and associates strength anisotropy, reaction kinetics, and thermal behavior. As such, the overall effects of microstructure are likely more pronounced than what is stated here. The current analysis should be regarded only as a first order estimate of the lower bound of the effects of microstructure relative to the effects of voids. We also note that only one relatively large void size (50 μm) is analyzed here. Void size is expected to affect the results [14, 35, 36]. Further studies should be carried out, accounting for more complete representations of material microstructure heterogeneities, as well as a range of void size, void volume fraction, and void morphologies. Ultimately, the effects of interfaces, cracks, and internal friction (see Refs. [15, 25]) should also be considered.

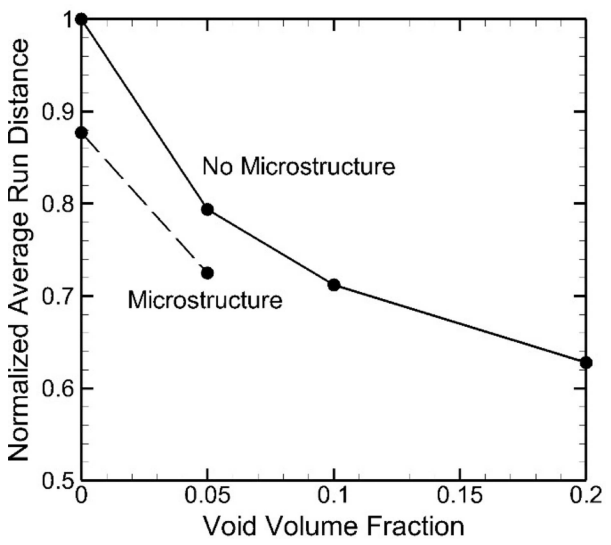

Figure 9. Normalized averaged decrease in run distance of samples with and without granular microstructure (dashed and solid lines respectively) as compared to homogeneous HMX as a function of void volume fraction.

3.3 Probabilistic Pop Plot Model

Up until now, the discussions regarding the rank-ordering of the effects of different microstructural attributes on SDT behavior have focused on the best curve fit associated with each Pop plot data set. This takes the form of a single line that represents the "average" behavior or trend. The analysis does not account for the fact that the behavior of HEM are stochastic due to several factors, the most important of which is intrinsic material heterogeneities at lower scales. The behavior of individual samples scatter around the overall trend line and the type and extent of heterogeneities determine the statistical spread and the uncertainties involved. There is a strong need to quantify not only the overall "average" behavior, but also the statistical distribution of the material behavior. The quantification must allow the uncertainties associated with SDT behavior assessment to be determined. Here, we use the SEMSS and the statistical SDT data sets obtained from the SEMSS to develop a probabilistic formulation for the Pop plot itself. To begin, each set of Pop plot data is fit to the standard power law

$$x^* = SP_s^{-m}, \tag{7}$$

where S is a material-dependent scaling parameter, m is an exponential fitting parameter, x^* is the run distance, and P_s is the shock pressure. This standard method Pop plot line represents the threshold of having 50% of the samples in a data set achieve SDT by a given run distance at a given pressure. In order to capture the probabilistic behavior of the Pop plot data set and quantify the likelihood of observing SDT at other combinations of run distance and shock pressure away from this line, a modified form of Eq. (7) is proposed with the introduction of a new, non-dimensional parameter D in the form of

$$D = \frac{(P_s - P_0)^m \left(x^* - x_0^*\right)}{S}. \tag{8}$$

This parameter can be regarded as the Pop plot characteristic number or the Pop plot number (PPN). It provides a measure of deviation from the 50% trend line of Eq. (7) in the run distance vs. shock pressure space, with $D > 0$. In particular, $D > 0$. represents the threshold where 50% of

the samples reach detonation (i.e., the traditional PP line); and $D < 1$ and $D < 1$ correspond to conditions for attaining SDT at greater than 50% and less than 50% probabilities, respectively. P_0 is the shock pressure below wich no SDT occurs, and x_0^* is the minimum run distance for observing SDT. These quantities can be regarded as material parameters which constitute bounds for P_s and x^*, respectively. Including these parameters allows the model to account for and separate conditions under which SDT may or may not occur. In particular, shock pressures that are too low may never lead to detonation (no go) as the applied energy disperses too quickly to form critical hotspots. The minimum run distance x_0^*, on the other hand, recognizes the fact that chemical reactions cannot occur instantaneously. Unlike the S and m material parameters in Eq. (7), the values for P_0 and x_0^* cannot be accurately predicted by fitting Eq. (8) to the data set here, as the calculations carried out here do not concern the physical conditions for these parameters. Instead, their values must be carefully determined based on independent experimental observations or separate computations with appropriate constitutive, EOS and chemistry models at both high and low shock pressures. That task is beyond the scope of this paper. According to the LASL explosive property database, the lowest recorded pressure tested for SDT is 4.41 GPa [37]. Low density HMX (65% TMD), which is known to be more sensitive than 100% TMD HMX, has been observed to reach SDT at shock pressures as low as 400 MPa [38]. Welle et al. calculated a minimum possible power flux required for ignition of class III pressed HMX samples of 0.35 GW/cm^2 [9]. Using the basic dynamic pressure equations, this minimum flux value roughly corresponds to a shock pressure of 2.26 GPa. Due to the lack of experimental data required to provide an accurate value for either P_0 or x_0^*, they are treated as insensitive fitting parameters in this paper. An accurate calibration of both parameters is required for future work in either the high or low pressure regime. If and when such data is obtained, they can be used to demarcate the domain in the shock pressure – run distance space in which the probabilistic analyses below can be more accurately used. Within that domain, these parameters have negligible bearing on the accuracy or validity of the analyses here.

The PPN offers a mechanism to quantitatively determine the probability of reaching SDT at any given point in the entire run distance and shock pressure space (the Pop plot space). Under the assumption that the distribution of data points in each data set follows a log-normal distribution about the line of Eq. (7), D can be used to obtain the cumulative probability of observing SDT in the form of

$$\mathscr{P}(D) = \frac{1}{\sigma_d\sqrt{2\pi}}\int_0^D \frac{1}{x}\exp\left[\frac{-(\ln x-\mu)^2}{2\sigma_d^2}\right]dx, \tag{9}$$

where μ is the mean of the natural logarithm of the PPN, and σ_d is the standard deviation of the spread of all data points in a given set around the 50% mean represented by Eq. (7). A log-normal distribution is chosen as it ensures the probability is symmetric about the PP line in log-log space. Since the mean value of the PPN is unit by definition, Eq. (9) may be simplified to

$$\mathscr{P}(D) = \frac{1}{\sigma\sqrt{2\pi}}\int_0^D \frac{1}{x}\exp\left[\frac{-(\ln x)^2}{2\sigma_d^2}\right]dx. \tag{10}$$

This may be rewritten as

$$\mathscr{P}(D) = \frac{1}{2}+\frac{1}{2}\mathrm{erf}\left(\frac{\ln D}{\sqrt{2}\sigma_d}\right), \tag{11}$$

where $\mathscr{P}$ is the probability of reaching SDT and D determines the location in the Pop plot space via Eq. (8). The fit for the homogeneous with 5% voids (V) SDT data set is shown in Figure 10. The material parameters for all data sets are shown in Table 6.

The form of Eq. (11) mirrors the probabilistic ignition threshold proposed by Kim et al. [15], which was initially based on the J parameter (the James number) first proposed by Gresshoff and Hrousis [39]. Here, the Pop plot

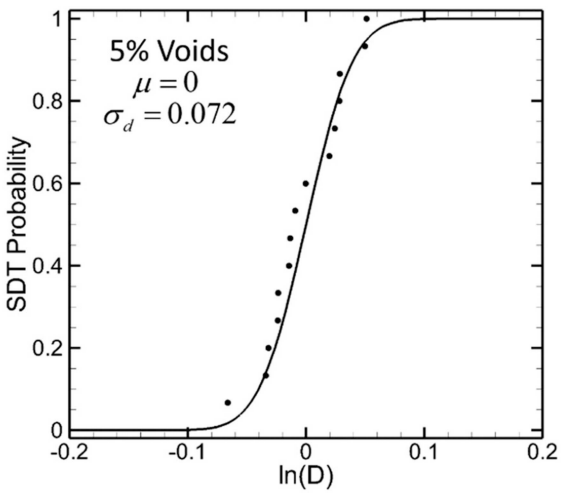

Figure 10. Cumulative SDT Probability as a function of the natural logarithm of the Pop plot number, D, for homogeneous samples with 5% voids (V). The data set is fit to Eq. (11).

Table 6. Probabilistic material parameters for all cases of HMX.

Sample Type/ Material Parameter	σ_d	S	m
Homogeneous (H)	0.024	73.5	1.80
Microstructure (M)	0.094	62.0	1.78
5% Voids (V)	0.072	58.2	1.84
5% Voids + Microstructure (V + M)	0.179	56.6	1.93

number D resembles the J parameter used by Kim et al. Substituting Eq. (8) into Eq. (11) gives the probability function in terms of the run distance and shock pressure, i.e.,

$$\mathscr{P}(P_s, x^*) = \frac{1}{2} + \frac{1}{2}\mathrm{erf}\left[\frac{1}{\sqrt{2}\sigma_d}\left(\ln\left(\frac{(P_s - P_0)^m (x^* - x_0^*)}{S}\right)\right)\right]. \quad (12)$$

In the above expression, $\mathrm{erf}(\cdot)$ is the error function. Using Eq. (12), we can generate a probability map for the entire Pop plot space of shock pressures and run distance for each material case. The resulting probability maps for the four materials cases analyzed are shown in Figure 11. These SDT probability distribution maps are the first of their kind and provide a systematic and quantitative means for predicting the probability of observing SDT at any combination of run distance and shock pressure. This analytical form can be used to guide experiments and selection of material by quantitatively relating common macroscopic measures. It is useful to point out that σ_d, m, and S in Eq. (12) are material parameters that are determined by the data set (obtained computationally or experimentally) for each material case. Ultimately, they can and should be expressly written as functions of material attribute measures such as constitutive properties, grain size, grain volume fraction, void content/size, and interfacial properties. Such an endeavor is not undertaken here, but the framework developed here lends itself to such future development.

Recently, Wei et al. extended this probabilistic approach from the James space for ignition thresholds to the Pop plot space for detonation thresholds [40]. We further expand upon it by recognizing that the SDT probability itself may serve as an input parameter for evaluating other quantities of interest in different design or materials selection scenarios. While Eq. (12) is useful in determining the likelihood of observing SDT for a given combination of shock pressure and run distance, it may also be used to calculate necessary conditions needed in order to reach a desired probability of detonation at a particular run distance or shock pressure. Specifically, the relation can be recast in the following form for calculating the minimum run distance required for achieving SDT with a given level of probability under a particular shock pressure

$$x^*(\mathscr{P}, P_s) = \frac{S}{(P_s - P_0)^m}\exp\left[\sqrt{2}\sigma_d(\mathrm{erf}^{-1}(2\mathscr{P} - 1))\right] + x_0^*. \quad (13)$$

In the above relation, $\mathrm{erf}^{-1}(\cdot)$ is the inverse error function, which approaches negative infinity at $\mathscr{P} = 0$ and positive infinity at $\mathscr{P} = 1$. There is no convenient closed form expression and is generally calculated numerically. The rela-

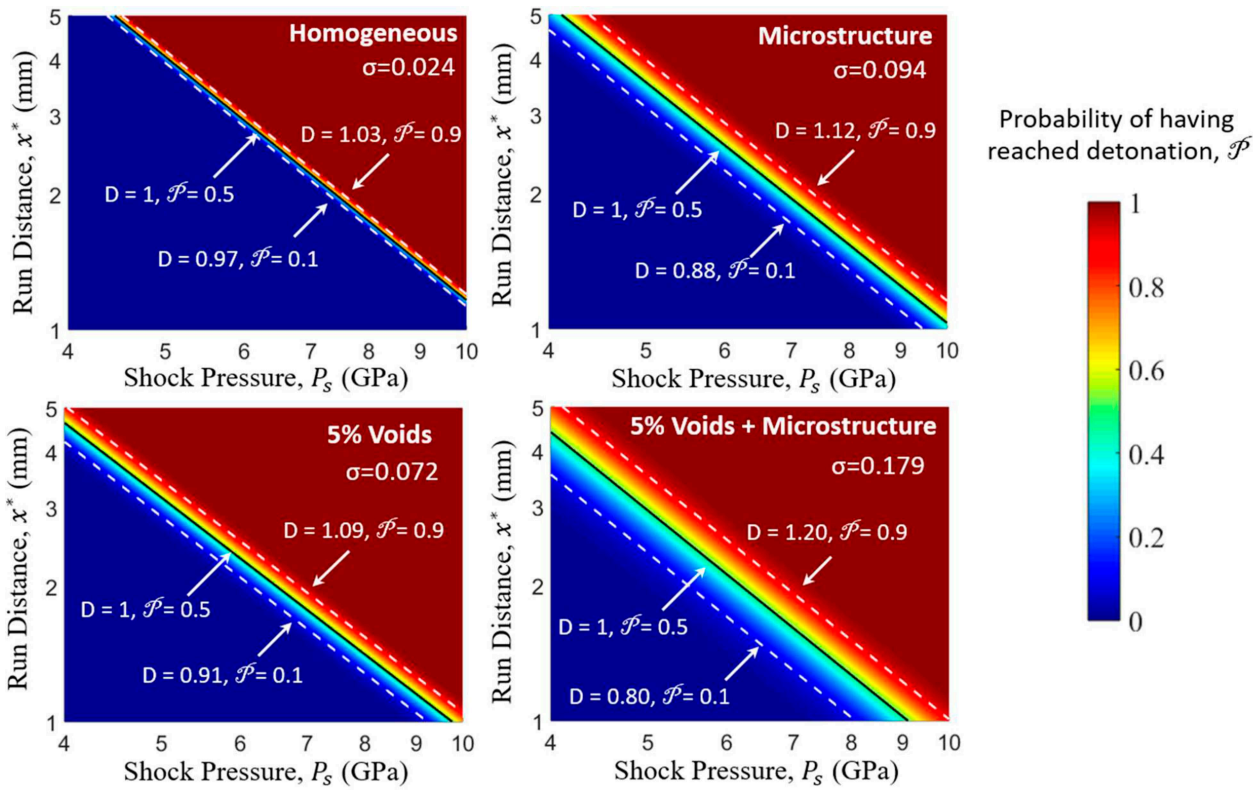

Figure 11. SDT probability distribution maps for the four cases of HMX analyzed: homogeneous (top left), microstructure (top right), 5% voids only (bottom left), and both voids and microstructure (bottom right).

tionship described by Eq. (13) has been mapped out over shock pressures ranging from 4–10 GPa and is shown in Figure 12 for the four material cases analyzed.

Similarly, the shock pressure required to achieve SDT at a specific run distance at a required probability is

$$P_s(\mathscr{P}, x^*) = \left\{ \frac{S}{(x^* - x_0^*)} \exp\left[\sqrt{2}\sigma_d (\mathrm{erf}^{-1}(2\mathscr{P} - 1)) \right] \right\}^{\frac{1}{m}} + P_0. \quad (14)$$

This relationship has been mapped out over the run distance range of 1–5 mm for the four material cases, and the result is shown in Figure 13. Both Eq. (13) and Eq. (14) result from simple algebraic manipulations of Eq. (12).

3.4 Experimental Comparison

A look at the prediction presented here in the context of available experimental data is in order and helpful. Figure 14 compares the results from section 3.1 with reported experimental Pop plot results for HMX (86% TMD) from Lawrence Livermore National Lab (LLNL) [38] and fully packed HMX (100% TMD) from Los Alamos National Lab (LANL) [37]. The results here are in general agreement with the experimental data in terms of overall trend. Only the 50% lines are shown, as there is a lack of statistical quantification in the experimental data sets. The decreasing of the predicted Pop plot lines as heterogeneities increase is consistent with the trend in the experimental data (density decreases). This is a first attempt at predicting the macroscopic PP using ME and VE mesoscale models. It is important to bear in mind the challenges in comparing such simulations to experiments. First, there are wide variations among the different experimental data sets. Possible reasons include material sample differences and inconsistencies (different batches of materials prepared at different times and locations can be significantly different), lack of quantification of the grain size distribution, void content, and statistical variations of these attributes, and experimental loading condition differences (different types of flyers, shock pressure and run distance measurement errors, etc.). Second, like any model, the model used here includes simplifications and assumptions, including the use of the specific HVRB chemistry model. With these factors in mind, we see that the simulations show that the homogeneous HMX case has a Pop plot line that is below that of the experimentally reported 100% TMD material. The exact cause of this discrepancy should be analyzed in future work. We

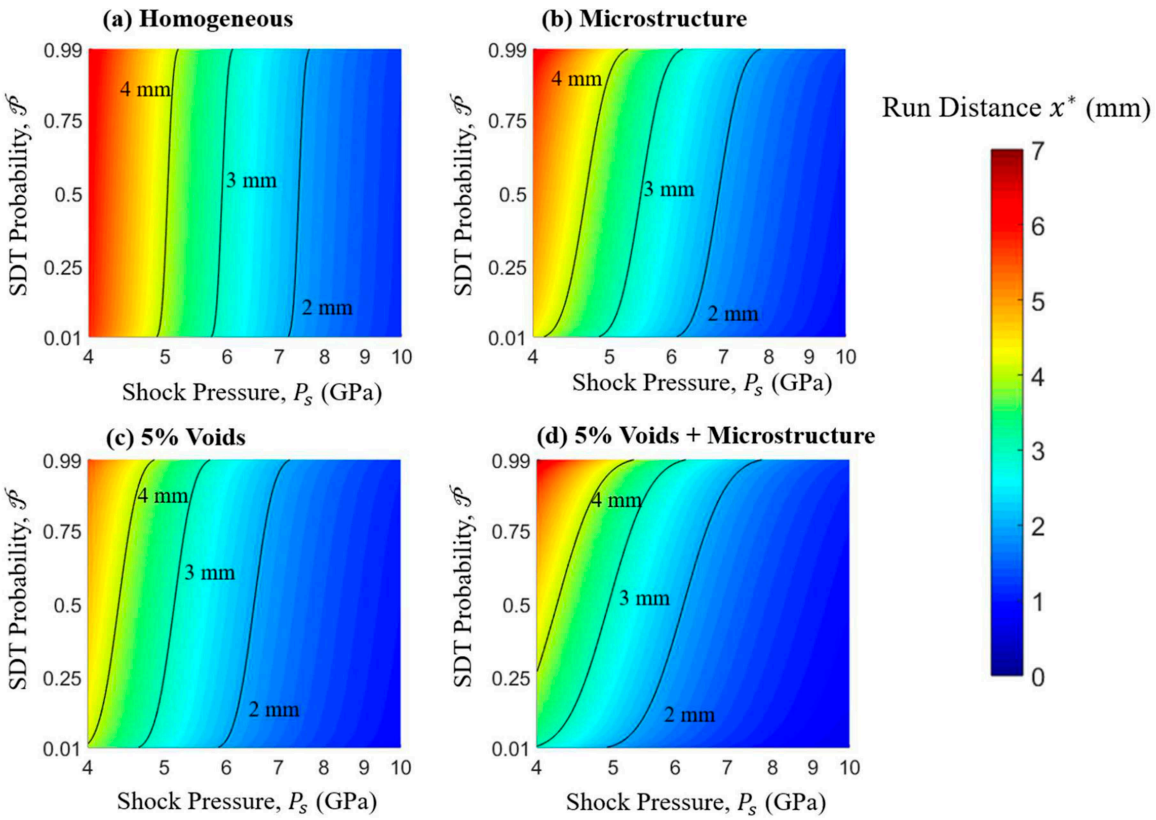

Figure 12. Necessary run distance to achieve a desired SDT probability under a given shock pressure for the four cases of HMX analyzed: (a) homogeneous, (b) microstructure, (c) 5% voids only, and (d) both voids and microstructure.

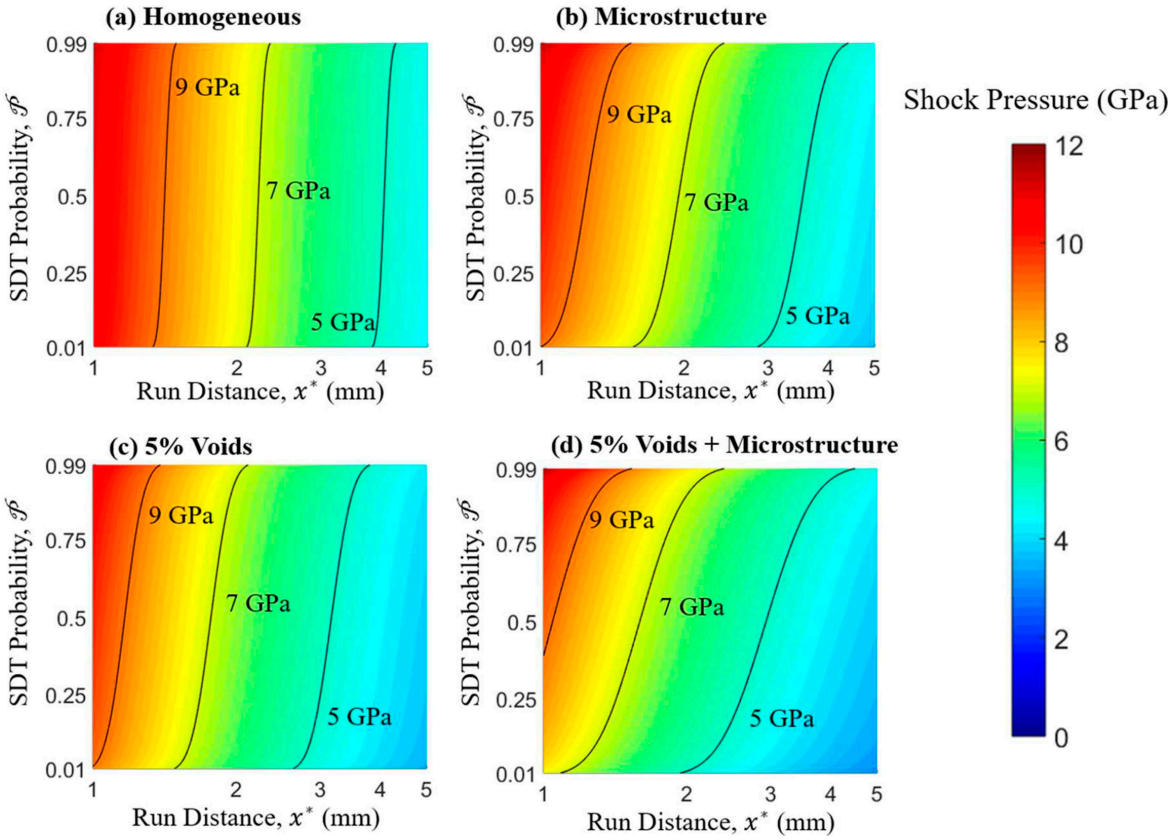

Figure 13. Necessary shock pressure to achieve a desired SDT probability at a given run distance for the four cases of HMX analyzed: (a) homogeneous, (b) microstructure, (c) 5% voids only, and (d) both voids and microstructure.

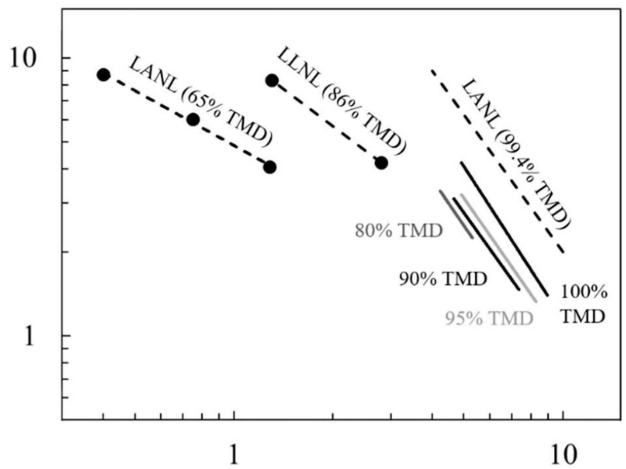

Figure 14. Comparison of the predicted Pop plot lines (solid lines) with available experimental data in the literature (dash lines). The predicted lines shown are for homogeneous HMX (H) and HMX with 5%, 10%, and 20% voids by volume (V).

surmise that this may be the result of limiting the computational analysis to a 2D plane strain model and the calibration of the HVRB used. We see this paper as only a first attempt at modeling the behavior of HMX at the macroscale with explicit account of both voids and microstructure. More localized material factors and processes are not explicitly resolved, and may account for some of the discrepancies seen between the simulations and experiments. Note also that the samples with a 5% void volume fraction (V and M+V) approximately correspond to the 95% TMD HMX in the experiments, with the understanding that detailed microstructure analyses were not reported in the references cited.

4 Conclusion

We have presented a mm-scale model for analyzing the SDT behavior of heterogeneous energetic materials. The model samples are microstructure-explicit, void-explicit, and large enough (mm length scale) to track the largest material size scale and SDT behavior size scale for common polymer-bonded explosives and granular explosives. The SDT behaviors of homogeneous HMX, HMX with granular microstructure, HMX with voids, and HMX with both granular microstructure and voids are analyzed and rank-ordered. The full transition from hotspot initiation to deto-

nation is simulated using an Eulerian computational framework which resolves the material heterogeneity and the coupled thermal-mechanical-chemical processes underlying the response of energetic materials under shock loading.

Simulations carried out show that adding a 5% volume fraction of voids to an otherwise homogeneous material decreases the average run distance by 20.6%. On the other hand, increasing the void volume fraction from 5% to 20% shortens the run distance by 37.2% relative to the homogeneous case. The heterogeneous microstructure also plays an important role in affecting the SDT behavior, causing the average run distance to decrease by 12.3% relative to the homogenous material. When both microstructure and voids are present, the average run distance decreases by another 6.9% over that of the material with 5% voids by volume. The results show that both voids and microstructure significantly affect the SDT process and the SDT thresholds. Further, as sources of heterogeneities, the effects of microstructure and voids on the SDT behavior are additive and interactive, implying that both must be considered and one cannot be used to account for the effects of the other. It is useful to bear in mind that the representation and resolution of microstructure heterogeneities are relatively simple and not exhaustive. Actual effects of microstructure are likely larger. The effects of void size are not explored in this paper.

A probabilistic formulation for quantifying the Pop plot is developed. This relation is general in nature and applicable to any type of HEM. It provides a useful framework for analyzing, selecting, and designing HEM. The relationship (Eq. (12)) can be used to determine the probability of observing the SDT at a given shock pressure and run distance. If a specific probability of SDT is desired, Eqs. (13) and (14) may be used to determine the necessary shock pressure or run distance, respectively. Ultimately, parameters in these relations can and should be expressed as functions of material constituent properties and microstructure attributes.

Finally, it is useful to point out that the goal of this paper is to illustrate the relative importance of two dominate microstructural aspects on the SDT process. This study is one of the first to quantify the relative effects of grains and voids using an Eulerian framework. While only the detonation behavior of pressed HMX is studied here, the effects of binder and additives in composite PBXs are still a main focus of the energetics community. The SDT probability study presented here can be expanded to other energetic compositions in the future.

Acknowledgements

Support from DTRA (grant HDTRA1-18-1-0004) and the Sandia LDRD AA program is gratefully acknowledged. CM also acknowledges support from the DoE NNSA Stewardship Science Graduate Fellowship Program (DE-NA0003864.). Any subjective views or opinions that might be expressed in the paper do not necessarily represent the views of the U.S. Department of Energy or the United States Government. Sandia National Laboratories is a multi-mission laboratory managed and operated by National Technology and Engineering Solutions of Sandia, LLC, a wholly owned subsidiary of Honeywell International, Inc., for the U.S. Department of Energy's National Nuclear Security Administration under contract DE-NA0003525.

References

[1] A. W. Campbell, Shock Initiation of Solid Explosives, *Phys. Fluids* **1961**, *4*, 511–521.
[2] R. L. Gustavsen, S. A. Sheffield, R. R. Alcon, Measurements of Shock Initiation in the Tri-Amino-Tri-Nitro-Benzene Based Explosive Pbx 9502: Wave Forms from Embedded Gauges and Comparison of Four Different Material Lots, *J. Appl. Phys.* **2006**, *99*, 114907.
[3] A. W. Campbell, W. C. Davis, J. R. Travis, Shock Initiation of Detonation in Liquid Explosives, *Phys. Fluids* **1961**, *4*, 498–510.
[4] S. A. Sheffield, *Shock Initiation and Detonation Study on High Concentration H2o2/H2o Solutions Using in-Situ Magnetic Gauges*, Report Los Alamos National Lab.(LANL), Los Alamos, NM (United States) **2010**.
[5] C. H. Johansson, P.-A. Persson, *Detonics of High Explosives.* Academic Press, London, **1970**.
[6] C. L. Mader, *Numerical Modeling of Explosives and Propellants.* 2nd ed.: CRC press, Boca Rato,**1998**.
[7] J. N. Johnson, P. K. Tang, C. A. Forest, Shock-Wave Initiation of Heterogeneous Reactive Solids, *J. Appl. Phys.* **1985**, *57*, 4323–4334.
[8] F. P. Bowden, A. D. Yoffe, *Initiation and Growth of Explosion in Liquids and Solids*. Cambridge University Press, **1952**.
[9] E. J. Welle, Microstructural Effects on the Ignition Behavior of Hmx, *J. Phys. Conf. Ser.* **2014**, *500*, 052049.
[10] M. R. Baer, Modeling Heterogeneous Energetic Materials at the Mesoscale, *Thermochim. Acta* **2002**, *384*, 351–367.
[11] C. L. Mader, Initiation of Detonation by the Interaction of Shocks with Density Discontinuities, *The Physics of Fluids* **1965**, *8*, 1811–1816.
[12] R. A. Austin, Direct Numerical Simulation of Shear Localization and Decomposition Reactions in Shock-Loaded Hmx Crystal, *J. Appl. Phys.* **2015**, *117*, 185902.
[13] C. A. Handley, Understanding the Shock and Detonation Response of High Explosives at the Continuum and Meso Scales, *Applied Physics Reviews* **2018**, *5*, 011303.
[14] N. K. Rai, H. S. Udaykumar, Mesoscale Simulation of Reactive Pressed Energetic Materials under Shock Loading, *J. Appl. Phys.* **2015**, *118*, 245905.
[15] S. Kim, Computational Prediction of Probabilistic Ignition Threshold of Pressed Granular Octahydro-1,3,5,7-Tetranitro-1,2,3,5-Tetrazocine (Hmx) under Shock Loading, *J. Appl. Phys.* **2016**, *120*, 115902.
[16] S. Kim, Prediction of Shock Initiation Thresholds and Ignition Probability of Polymer-Bonded Explosives Using Mesoscale Simulations, *J. Mech. Phys. Solids* **2018**, *114*, 97–116.
[17] T. L. Jackson, Multi-Dimensional Mesoscale Simulations of Detonation Initiation in Energetic Materials with Density-Based Kinetics, *Combust. Theory Modell.* **2018**, *22*, 291–315.
[18] M. A. Wood, Multiscale Modeling of Shock Wave Localization in Porous Energetic Material, *Phys. Rev. B* **2018**, *97*, 014109.
[19] C. D. Yarrington, R. R. Wixom, D. L. Damm, Shock Interactions with Heterogeneous Energetic Materials, *J. Appl. Phys.* **2018**, *123*, 105901.

[20] J. M. McGlaun, S. L. Thompson, M. G. Elrick, Cth: A Three-Dimensional Shock Wave Physics Code, *Int J Impact Eng* **1990**, *10*, 351–360.
[21] J. J. Dick, The Hugoniot and Shock Sensitivity of a Plastic-Bonded Tatb Explosive Pbx 9502, *J. Appl. Phys.* **1988**, *63*, 4881–4888.
[22] J. R. Peterson, C. A. Wight, M. Berzins, Applying High-Performance Computing to Petascale Explosive Simulations, *Procedia Computer Science* **2013**, *18*, 2259–2268.
[23] J. Starkenberg, T. M. Dorsey, *An Assessment of the Performance of the History Variable Reactive Bum Explosive Initiation Model in the Cth Code*, Report ARL-TR-1667, Army Research Lab, Aberdeen Proving Ground, MD, USA **1998**.
[24] D. B. Hardin, J. J. Rimoli, M. Zhou, Analysis of Thermomechanical Response of Polycrystalline Hmx under Impact Loading through Mesoscale Simulations *K AIP Adv.* **2014**, *4*, 097136.
[25] Y. Wei, Quantification of Probabilistic Ignition Thresholds of Polymer-Bonded Explosives with Microstructure Defects, *J. Appl. Phys.* **2018**, *124*, 165110.
[26] K. Ramos, M. Cawkwell, D. Hooks, Defect Characterization and the Effect of Pre-Existing and Shock-Induced Defects on the Shock Response of Single Crystal Explosives. in *17th Biennial International Conference of the APS Topical Group on Shock Compression of Condensed Matter*. Chicago, Illinois **2011**.
[27] C. Hua, Research on the Size of Defects inside Rdx/Hmx Crystal and Shock Sensitivity, *Propellants Explos. Pyrotech.* **2013**, *38*, 775–780.
[28] C. Miller, Ignition Thresholds of Aluminized Hmx-Based Polymer-Bonded Explosives, *AIP Adv.* **2019**, *9*, 045103.
[29] E. L. Lee, C. M. Tarver, Phenomenological Model of Shock Initiation in Heterogeneous Explosives, *Phys. Fluids* **1980**, *23*, 2362–2372.
[30] R. Menikoff, M. S. Shaw, Reactive Burn Models and Ignition & Growth Concept, *Epj Web Conf.* **2010**, *10*.
[31] R. Schmitt, Cth User's Manual and Input Instructions Version 11.2. *CTH Development Project, Sandia National Laboratories, Albuquerque, NM*, **2016**.
[32] G. I. Kerley, Cth Equation of State Package: Porosity and Reactive Burn Models. *Sandia National Laboratories report SAND92-0553*, **1992**.
[33] R. Menikoff, T. D. Sewell, Constituent Properties of Hmx Needed for Meso-Scale Simulaitons. *Los Alamos National Lab.*, **2001**.
[34] N. J. Burnside, Particle Characterization of Pressed Granular Hmx, *Shock Compression of Condensed Matter*. **1997**, *571*.
[35] S. D. Herring, T. C. Germann, N. Grønbech-Jensen, Effects of Void Size, Density, and Arrangement on Deflagration and Detonation Sensitivity of a Reactive Empirical Bond Order High Explosive, *Phys. Rev. B*, **2010**, *82*, 214108.
[36] C. Yarrington, R. R. Wixom, D. L. Damm, *Mesoscale Simulations Using Realistic Microstructure and First Principles Equation of State*, Report SAND2012-9583 C, Sandia National Lab.(SNL-NM), Albuquerque, NM (United States) **2012**.
[37] T. R. Gibbs, A. Popolato, *Lasl Explosive Property Data*. University of California, Berkeley.**1980**.
[38] F. Garcia, K. S. Vandersall, C. M. Tarver, Shock Initiation Experiments with Ignition and Growth Modeling on Low Density Hmx, *J. Phys. Conf. Ser.* **2014**, 052048.
[39] M. Gresshoff, C. A. Hrousis. Probabilistic Shock Threshold Criterion. in *14th International Detonation Symposium*. Coeur d'Alene, ID **2010**.
[40] Y. Wei, Integrated Lagrangian and Eulerian 3d Microstructure-Explicit Simulations for Predicting Macroscopic Probabilistic Sdt Thresholds of Energetic Materials. *Comput. Mech.* **2019**.

Manuscript received: June 24, 2019
Revised manuscript received: November 7, 2019
Version of record online: December 9, 2019

